

# First forbidden stellar $\beta$ -decay rates for neutron-rich nickel isotopes

Jameel-Un Nabi\*<sup>1</sup> and Sabin Stoica<sup>2</sup>

<sup>1</sup>*Faculty of Engineering Sciences, GIK Institute of Engineering Sciences and Technology,  
Topi 23640, Swabi, Khyber Pakhtunkhwa, Pakistan*

<sup>2</sup>*Horia Hulubei Foundation, P. O. Box MG-12, 071225, Magurele, Romania*

In astrophysical environments, allowed Gamow-Teller (GT) transitions are important, particularly for  $\beta$ -decay rates in presupernova evolution of massive stars, since they contribute to the fine-tuning of the lepton-to-baryon content of the stellar matter prior to and during the collapse of a heavy star. In environments where GT transitions are unfavored, first-forbidden transitions become important especially in medium heavy and heavy nuclei. Particularly in case of neutron-rich nuclei, first-forbidden transitions are favored primarily due to the phase-space amplification for these transitions. In this work the total  $\beta$ -decay half-lives and the unique first-forbidden(U1F)  $\beta$ -decay rates for a number of neutron-rich nickel isotopes,  $^{72-78}\text{Ni}$ , are calculated using the proton-neutron quasi-particle random phase approximation (pn-QRPA) theory for the first time in stellar matter. For the calculation of the  $\beta$ -decay half-lives both allowed and first-forbidden transitions were considered. Comparison of the total half-lives is made with measurements and other theoretical calculation. The pn-QRPA results agree reasonably well with experiments.

**PACS** numbers: 21.60.Jz, 23.40.Bw, 23.40.-s, 26.30.Jk, 26.50.+x

## I. INTRODUCTION

Reliable and precise knowledge of the  $\beta$ -decay for neutron-rich nuclei is crucial to an understanding of the r-process. Both the element distribution on the r-path, and the resulting final distribution of stable elements are highly sensitive to the  $\beta$ -decay properties of the neutron-rich nuclei involved in the process [1, 2]. There are about 6000 nuclei between the  $\beta$  stability line and the neutron drip line. Most of these nuclei cannot be produced in terrestrial laboratories and one has to rely on theoretical extrapolations in respect of beta decay properties. In neutron-rich environments electron neutrino captures could not only amplify the effect of  $\beta$ -decays but the subsequent  $\nu$ -induced neutron spallation can

---

\* Current Address: Horia Hulubei Foundation, P. O. Box MG-12, 071225, Magurele, Romania  
Corresponding author e-mail: jameel@giki.edu.pk

also contribute towards changing the r-abundance distribution pattern [3]. Correspondingly reliable predictions of  $\beta$ -decay for neutron-rich nuclei are considered to be very important for r-process nucleosynthesis.

The weak interaction rates are the important ingredients playing a crucial role in practically all stellar processes: the hydrostatic burning of massive stars, presupernova evolution of massive stars, and nucleosynthesis (s-, p-, r-, rp-) processes (see, for example, the seminal paper by Burbidge and collaborators [4]). For densities  $\rho \lesssim 10^{11} g/cm^3$ , stellar weak interaction processes are dominated by Gamow-Teller (GT) and, if applicable, by Fermi transitions. For nuclei lying in the vicinity of the line of stability, forbidden transitions contribute sizably for  $\rho \gtrsim 10^{11} g/cm^3$  when the electron chemical potential reaches values of the order of 30 MeV or more [5].

During presupernova stage of stellar evolution, electron capture dominates the weak interaction processes. However, after silicon depletion in the core and during the silicon shell burning,  $\beta$ -decay competes temporarily with electron capture and further cools the star. Unlike electron capture, the  $\beta$ -decay at silicon burning stage increases and this bears consequences because  $\beta$ -decays are additional neutrino source and add to the cooling of the stellar core and a reduction in stellar entropy. This cooling of stellar core can be quite efficient as often the average neutrino energy in the involved  $\beta$ -decays is larger than for the competing electron capture processes. Consequently, the  $\beta$ -decay lowers the stellar core temperature after silicon shell burning. For a discussion on the fine-tuning of lepton-to-baryon ratio of stellar matter during presupernova evolution see Ref. [6]. As the density of the stellar core increases the allowed  $\beta$ -decay becomes unimportant and hindered due to the fact that the increasing Fermi energy of electrons blocks the available phase space for the electron to be produced in the  $\beta$ -decay. (For a detailed discussion of the role of weak interaction in the presupernova evolution of massive stars see Ref. [7].) In case of neutron-rich nuclei, first-forbidden  $\beta$ -decay may become important due to the enlarge phase space for these transitions [8, 9].

Reliable, quantitative estimates of  $\beta$ -decay half-lives of neutron-rich nuclei are needed in astrophysics for the understanding of supernova explosions, and the processes of nucleosynthesis, particularly the r-process. The  $\beta$ -decay half-lives are also needed for the experimental exploration of the nuclear landscape at existing and future radioactive ion-beam facilities. The calculation of  $\beta$ -decay half-lives in agreement with experimental results has been a challenging problem for nuclear theorists.

Because of the scarcity of experimental data, majority of the  $\beta$ -decay rates of the neutron-rich nuclei have been investigated using theoretical models. Several models of different level of sophistication for determining  $\beta$ -decay half-lives have been proposed and applied over the years. One can mention the more phenomenological treatments based on Gross Theory (e.g. [10]) as well as microscopic treatments that employ the proton-neutron quasiparticle

random phase approximation (pn-QRPA) [11, 12] or the shell model [13]. The later hybrid version of the RPA models developed by Möller and coworkers, combines the pn-QRPA model with the statistical Gross Theory of the first forbidden decay (pnQRPA+ffGT)[14]. There are also some models in which the ground state of the parent nucleus is described by the Hartree-Fock BCS method, or other density functional method (DF) and which use the continuum QRPA (CQRPA) (e.g. [15]). Recently relativistic pn-QRPA (RQRPA) models have been applied in the treatment of neutron-rich nuclei in the  $N \sim 50$ ,  $N \sim 82$  and  $Z \sim 28$  and  $50$  regions [16, 17]. Despite continuing improvements the predictive power of these conventional models is rather limited for  $\beta$ -decay half-lives of nuclei.

The microscopic calculations of allowed weak interaction rates using the pn-QRPA model [11, 12, 18] and first-forbidden  $\beta$ -decay properties by Homma and collaborators [19] led to a better understanding of the r-process. However there was a need to go to domains of high temperature and density scales where the weak interaction rates are of decisive importance in studies of the stellar evolution.

Two different microscopic approaches, namely the shell model [20] and the pn-QRPA [21], have so far been successively used in the large-scale calculation of stellar weak-interaction mediated rates for r-process applications. Whereas the advantage of the shell model clearly lies in its ability to take into account the detailed structure of the  $\beta$ -strength functions, the shell model is forced to use approximations like Brink's hypothesis (in electron capture direction) and back resonances (in  $\beta$ -decay direction) when extending the calculation to high-lying excited states. These states can contribute rather significantly to the total weak rate in high temperature and high density environments. Brink's hypothesis states that GT strength distribution on excited states is *identical* to that from ground state, shifted *only* by the excitation energy of the state. GT back resonances are the states reached by the strong GT transitions in the inverse process (electron capture) built on ground and excited states. On the other hand the pn-QRPA model gets rid of such approximations and allows a state-by-state evaluation of the weak rates by summing over Boltzmann-weighted, microscopically determined GT strengths *for all* parent excited states.

In this paper we attempt to calculate the allowed as well as the unique first-forbidden (U1F)  $\beta$ -decay rates for neutron-rich nickel isotopes using the pn-QRPA model for the first time in stellar matter. Our calculations do not employ approximations (Brink's hypothesis and/or back resonances). The recent measurement of the  $GT_+$  strength distribution of  $^{76}\text{Se}$  [22] supports the argument that, due to nuclear correlations across the  $N = 40$  shell gap, the GT transitions for fp-nuclei with proton numbers  $Z < 40$  and neutron numbers  $N > 40$  would not be Pauli blocked. Nevertheless for neutron-rich nuclei U1F transitions are favored due to the amplification of available phase space. It is in this context that we attempt here to calculate both allowed GT and U1F transitions for neutron-rich nickel isotopes

( $^{72-78}\text{Ni}$ ). The theory of allowed and first-forbidden  $\beta$ -decay transitions (along with its leptonic phase-space content and nuclear matrix elements) is well-established [23–27]. Whereas the allowed  $\beta$ -decay (having the same parity before and after the decay) is relatively simple to calculate, the first-forbidden decay shows a far wider spectrum both in lepton kinematics and in nuclear matrix elements [23, 24, 27]. It is to be noted that in this work only the contribution of U1F to the calculated half-lives has been performed. The effects of non-unique forbidden transitions, for some nuclei, may have still larger contributions to the total half-lives and would be considered as a future project.

The pn-QRPA formalism for calculations of the total  $\beta$ -decay half-lives and U1F  $\beta$ -decay rates for neutron-rich nickel isotopes are discussed in section II. Results and comparisons with experimental and other theoretical calculation are shown in section III. Section IV outlines the importance of the results in connection with the simulation of the advanced stages of stellar evolution and nucleosynthesis and concludes our discussion on consequences of U1F  $\beta$ -decays in stellar matter.

## II. FORMALISM

In the pn-QRPA formalism [28], proton-neutron residual interactions occur in two different forms, namely as particle-hole (ph) and particle-particle (pp) interactions. The particle-hole and particle-particle interactions can be given a separable form because  $\beta^-$  transitions are dominated by the particle-hole interaction. These ph and pp forces are repulsive and attractive, respectively, when the strength parameters  $\chi$  for ph GT force and  $\kappa$  for pp GT force take positive values. The advantage of using these separable GT forces is that the QRPA matrix equation reduces to an algebraic equation of fourth order, which is much easier to solve as compare to full diagonalization of the non-Hermitian matrix of large dimensionality [19, 28].

Essentially we first construct a quasiparticle basis (defined by a Bogoliubov transformation) with a pairing interaction, and then solve the RPA equation with a schematic separable GT residual interaction. The single particle energies were calculated using a deformed Nilsson oscillator potential with a quadratic deformation. The pairing correlation was taken into account in the BCS approximation using constant pairing forces. The BCS calculation was performed in the deformed Nilsson basis for neutrons and protons separately. The formalism for calculation of allowed  $\beta$ -decay rates in stellar matter using the pn-QRPA model can be seen in detail from Refs. [21, 29]. Below we describe briefly the necessary formalism to calculate the U1F  $\beta$ -decay rates.

Allowed Fermi and GT transitions have a maximum spin change of one unit and no change in parity of the wavefunction. In contrast, the most frequent occurrence of a forbidden decay is when the initial and final states have

opposite parities, and thus the selection rule for allowed decay is violated. The spins of the initial and final states can be different at most by  $\Delta J = 0, \pm 1, \pm 2$ ; those with  $\Delta J = \pm 2$  are specified as being unique first-forbidden (U1F). The isospin selection rule remains the same as for allowed decays. For the calculation of the U1F  $\beta$ -decay rates, matrix elements of the separable forces which appear in RPA equation are given by

$$V_{pn,p'n'}^{ph} = +2\chi f_{pn}(\mu) f_{p'n'}(\mu), \quad (1)$$

$$V_{pn,p'n'}^{pp} = -2\kappa f_{pn}(\mu) f_{p'n'}(\mu), \quad (2)$$

where

$$f_{pn}(\mu) = \langle j_p m_p | t_{-r} [\sigma Y_1]_{2\mu} | j_n m_n \rangle \quad (3)$$

is a single-particle U1F transition amplitude (the symbols have their normal meaning). Note that  $\mu$  takes the values  $\mu = 0, \pm 1$ , and  $\pm 2$  (for allowed decay rates  $\mu$  only takes the values 0 and  $\pm 1$ ), and the proton and neutron states have opposite parities [19]. In this work we took  $\chi = 0.90 \text{ MeV}$  and  $\kappa = 0.01 \text{ MeV}$  for all nickel isotopes. Deformations of the nuclei were calculated using

$$\delta = \frac{125(Q_2)}{1.44(Z)(A)^{2/3}}, \quad (4)$$

where  $Z$  and  $A$  are the atomic and mass numbers, respectively and  $Q_2$  is the electric quadrupole moment taken from Ref. [30].  $Q$ -values were taken from the recent mass compilation of Audi et al. [31].

The U1F  $\beta$ -decay rates from the  $i$ th state of the parent to the  $j$ th state of the daughter nucleus is given by

$$\lambda_{ij} = \ln 2 \frac{f_{ij}(T, \rho, E_f)}{(ft)_{ij}}. \quad (5)$$

The phase-space factors  $f_{ij}$  are given as integrals over the lepton distribution functions and hence are sensitive functions of the temperature and density in stellar interior. The  $(ft)_{ij}$  are the comparative half-lives and are related to the U1F weak interaction matrix elements.

For the first forbidden transitions the integral can be obtained as

$$f_{ij} = \int_1^{w_m} w \sqrt{w^2 - 1} (w_m - w)^2 [(w_m - w)^2 F_1(Z, w) + (w^2 - 1) F_2(Z, w)] (1 - G_-) dw, \quad (6)$$

where  $w$  is the total kinetic energy of the electron including its rest mass and  $w_m$  is the total  $\beta$ -decay energy ( $w_m = m_p - m_d + E_i - E_j$ , where  $m_p$  and  $E_i$  are mass and excitation energies of the parent nucleus, and  $m_d$  and  $E_j$  of the daughter nucleus, respectively).  $G_-$  are the electron distribution functions. Assuming that the electrons are not in a bound state, these are the Fermi-Dirac distribution functions,

$$G_- = [\exp(\frac{E - E_f}{kT}) + 1]^{-1}. \quad (7)$$

Here  $E = (w - 1)$  is the kinetic energy of the electrons,  $E_f$  is the Fermi energy of the electrons,  $T$  is the temperature, and  $k$  is the Boltzmann constant.

The Fermi functions,  $F_1(\pm Z, w)$  and  $F_2(\pm Z, w)$  appearing in Eq. (6) are calculated according to the procedure adopted by Gove and Martin [32].

The number density of electrons associated with protons and nuclei is  $\rho Y_e N_A$ , where  $\rho$  is the baryon density,  $Y_e$  is the ratio of electron number to the baryon number, and  $N_A$  is the Avogadro's number.

$$\rho Y_e = \frac{1}{\pi^2 N_A} \left(\frac{m_e c}{\hbar}\right)^3 \int_0^\infty (G_- - G_+) p^2 dp, \quad (8)$$

where  $p = (w^2 - 1)^{1/2}$  is the electron or positron momentum, and Eq. (8) has the units of *moles cm*<sup>-3</sup>. This equation is used for an iterative calculation of Fermi energies for selected values of  $\rho Y_e$  and  $T$ .

There is a finite probability of occupation of parent excited states in the stellar environment as a result of the high temperature in the interior of massive stars. Weak decay rates then also have a finite contribution from these excited states. The occupation probability of a state  $i$  is calculated on the assumption of thermal equilibrium,

$$P_i = \frac{\exp(-E_i/kT)}{\sum_{i=1} \exp(-E_i/kT)}, \quad (9)$$

where  $E_i$  is the excitation energy of the state  $i$ , respectively. The rate per unit time per nucleus for any weak process is then given by

$$\lambda = \sum_{ij} P_i \lambda_{ij}. \quad (10)$$

The summation over all initial and final states are carried out until satisfactory convergence in the rate calculations is achieved.

### III. RESULTS AND COMPARISON

In this section we present the calculation of the total  $\beta$ -decay half-lives and U1F  $\beta$ -decay rates for neutron-rich Ni isotopes. Both allowed GT and U1F transitions are considered for calculations of the  $\beta$ -decay half-lives. The calculated half-lives are also compared with the measured ones to estimate the accuracy of the predicted decay rates.

For the Ni isotopic chains the results are shown in Fig. 1 and compared with experimental values [33–35] and with the self-consistent density functional + continuum quasiparticle random phase approximation (DF3 + CQRPA) calculation of Ref. [36].

The calculation performed in the present work is in better agreement with the experimental data. The inclusion of the first-forbidden transitions within the pn-QRPA results in noticeably shorter half-lives and satisfactory agreement with experiment is reached when first-forbidden transitions are included.

The pn-QRPA half-lives are slightly bigger than experimental half-lives [33] for  $^{72,73}\text{Ni}$  whereas the calculated half-lives of Ref. [36] are slightly smaller than the corresponding measured values. For the rest of the cases ( $^{74-78}\text{Ni}$ ) the pn-QRPA calculated half-lives are in excellent comparison with the measured half-lives. The calculation shows that the inclusion of the U1F contribution makes the half-life predictions more reliable for neutron-rich nickel isotopes.

Table 1 shows the available phase space for allowed and U1F transitions, as a function of stellar temperature and density, for the neutron-rich nickel isotopes. The phase space is calculated at selected density of  $10^2 \text{ g/cm}^3$ ,  $10^6 \text{ g/cm}^3$ ,  $10^{10} \text{ g/cm}^3$  (corresponding to low, intermediate and high stellar densities, respectively) and stellar temperature  $T_9 = 0.01, 1, 3$  and  $10$  ( $T_9$  gives the stellar temperature in units of  $10^9 \text{ K}$ ). It can be seen from this table that for high densities the phase space increases with increasing stellar temperature. As the stellar core becomes more and more dense the phase space decreases. The phase space increases by 1-3 orders of magnitude for U1F transitions. This enlarged phase space makes the U1F  $\beta$ -decay rates significant for the neutron-rich isotopes as will be discussed below.

The U1F  $\beta$ -decay rates were calculated for densities in the range  $10^{0.5}-10^{11} \text{ g/cm}^3$  and temperature range  $0.01 \leq T_9 \leq 30$ . Figs. 2- 8 show three panels depicting pn-QRPA calculated allowed and U1F  $\beta$ -decay rates at selected temperature and density domain for chosen neutron-rich nickel isotopes. The total  $\beta$ -decay rates are a sum of these two contributions. Fig. 2 depicts stellar  $\beta$ -decay rates for  $^{72}\text{Ni}$  in units of  $\text{sec}^{-1}$ . It is pertinent to mention that contribution from all excited states are included in the final calculation of all decay rates. It can be seen from this figure that for low and intermediate densities ( $10^2$  and  $10^6 \text{ g/cm}^3$ ) the  $\beta$ -decay rates (both allowed and U1F) remain almost the same as a function of stellar temperature. At low temperatures ( $T_9 \leq 5$ ) the U1F transition is an order of magnitude bigger than the allowed transition primarily because of the enlarged phase space as shown in Table 1.

At high stellar temperatures the allowed transitions become dominant as more and more excited states contribute significantly to the allowed GT rates. For these high stellar temperatures the allowed GT rates are bigger than the U1F rates roughly by a factor of five. At high stellar density ( $10^{10}$  g/cm<sup>3</sup>) the  $\beta$ -decay rates tend to go down due to the blocking of the available phase space of increasingly degenerate electrons. At high densities and high temperatures the contribution to the total  $\beta$ -decay rates by the excited states is very important. The rates rise with higher temperature as more excited states start contributing when the temperature increases. Increasing temperature and density have opposite contributions to the calculated rates. Whereas growth of the stellar density suppresses the  $\beta$  decay rates due to a diminishing phase space available for escaping electrons, increase in temperature weakens the Pauli blocking and therefore enhances the contribution of the GT<sub>-</sub> transitions from excited states of the parent nucleus.

Figs. 3, 4 and 5, show the cases of <sup>73</sup>Ni, <sup>74</sup>Ni and <sup>75</sup>Ni, respectively. The results almost follow the same trend as shown in Fig. 2. The U1F  $\beta$ -decay rates continue to dominate till still higher temperatures ( $T_9 \sim 20$ ) for the case of <sup>74</sup>Ni and <sup>75</sup>Ni (for low and intermediate densities). At high stellar temperatures,  $T_9 \sim 30$ , the allowed GT rates dominate. The effects of increasing temperature and density on the decay rates were discussed earlier.

Fig. 6 shows a different behavior for the case of <sup>76</sup>Ni. Here the U1F rates are bigger than the allowed rates for all temperatures at low and intermediate densities. The U1F rates are more than an order of magnitude bigger at low temperatures. At high temperatures the two rates tend to approach each other with the U1F rate still slightly bigger. At high densities the U1F rates are almost three orders of magnitude bigger at low temperatures. As the temperature increases the allowed GT rates tend to increase at a faster rate and at  $T_9 = 30$ , the allowed rates is almost double the U1F rate. The reason for this new trend can be traced back partly due to the phase space calculation (see Table 1) where the U1F phase space is much bigger than the allowed phase space and partly due to calculation of much larger values for U1F transition amplitudes (nuclear matrix elements).

Fig. 7 (<sup>77</sup>Ni) follows the normal trend. One notes that for the case of <sup>77</sup>Ni, for low and intermediate densities, the U1F rates dominate up till  $T_9 \sim 25$ . For the case of <sup>78</sup>Ni it can be seen from Fig. 8 that at high densities and low temperatures the U1F rates are up to two orders of magnitude bigger. As temperature increases the allowed rates overtake the U1F rates and at  $T_9 = 30$  they are almost three times bigger. The reason for this behavior is again traced back to phase space calculation for U1F transition of <sup>78</sup>Ni (see Table 1). At high densities the phase space is around three orders of magnitude bigger for the U1F transition and explains the orders of magnitude bigger U1F  $\beta$ -decay rates. Increasing the stellar temperature weakly affects the U1F  $\beta$ -decay rates. The reason is that the first forbidden transitions are of relatively high energies and basically of the particle-hole nature. Therefore a smearing of



single-particle strengths due to pairing correlations and temperature influence them considerably less. On the other hand the allowed GT rates increase at a faster pace with increasing temperature and hence explains this feature in all figures.

In the  $\beta$ -decay of a particular isotope, an emitted electron can receive any kinetic energy from zero up to the maximum kinetic energy available for the decay. In stellar environments, the electron density can be sufficiently high so that the low-energy states of the electron gas are essentially filled. In such an environment, there are fewer states available into which a low-energy electron can be emitted, and therefore  $\beta$ -decay is strongly inhibited if maximum kinetic energy available for the decay is small. The  $\beta$ -decay rate of an isotope depends on the local temperature, the local density, the maximum  $\beta$ -decay energy of the isotope, and the of  $\beta$ -decay process involved [37]. For U1F decays (parity changes and  $\Delta J = \pm 2$ ), when maximum kinetic energy available for the decay is small, the inhibition of first-forbidden unique decays is not as large as the inhibition of allowed, for the same temperature, density, and  $\beta$ -decay energy [36].

#### IV. CONCLUSIONS

In this work the total stellar  $\beta^-$ -decay half-lives and U1F  $\beta$ -decay rates for a number of neutron-rich nuclei have been calculated, for the first time, using the pn-QRPA theory. The temperature and density profiles were relevant to the advanced nuclear burning stages of the presupernova and supernova star. The results for total  $\beta$ -decay half-lives are in good agreement with the experimental results [33–35].

The microscopic calculation of U1F  $\beta$ -decay rates, presented in this work, could lead to a better understanding of the nuclear composition and  $Y_e$  in the core prior to collapse. These calculated rates are also required in calculations of the hydrostatic phases of presupernova evolution through core silicon burning and the onset of core collapse and hence are required for an understanding of the explosion mechanism. It has been found that the inclusion of accurate weak rates during all stages of nuclear burning, from core oxygen burning onwards, leads to an important difference in presupernova iron core structure and its entropy prior to core collapse.

What impact enhanced U1F  $\beta$ -decay rates may have on core collapse simulation results? The effects of enhanced U1F  $\beta$ -decays are two-fold. These enhanced rates on neutron-rich nuclei significantly increase the value of  $Y_e$  as compared to allowed  $\beta$ -decay rates after oxygen depletion and during silicon shell burning in stellar core. The increment in  $Y_e$  during and after silicon shell burning is primarily due to the increased phase space for the  $\beta$ -decay electrons and should be more for the reported U1F  $\beta$ -decay rates. Secondly,  $\beta$ -decays are additional neutrino sources and contribute

to the cooling of the stellar core and to the reduction in entropy. The lower entropy favors the explosion mechanism. The enhanced cooling of the core due to U1F  $\beta$ -decay rates of neutron-rich nuclei will be quite efficient, because the average energies of the neutrinos emitted in the U1F  $\beta$ -decays will be bigger than the allowed  $\beta$ -decay rates and also for the competing allowed electron captures. As a consequence, the U1F  $\beta$ -decay rates lead to a significantly lower core temperature during and after silicon.

During the collapse phase allowed  $\beta$ -decays become unimportant due to the increased electron chemical potential which drastically reduces the phase space for the beta electrons. It is well known that a smaller lepton fraction disfavors the outward propagation of the post-bounce shock waves, as more overlying iron core has to be photo-dissociated. It is noted that the U1F  $\beta$ -decay rates yield higher  $Y_e$  in comparison to allowed  $\beta$ -decay rates prior to collapse. This might assist the march of post-bounce shock for a successful supernova explosion to occur. These stronger  $\beta$ -decay rates can also assist in a more vigorous URCA process and lead to cooler presupernova cores consisting of lesser neutron-rich matter than in presently assumed core-collapse simulations. The allowed and U1F  $\beta$ -decay rates were calculated on a fine temperature-density grid, suitable for simulation codes, and may be requested as ASCII files from the corresponding author.

The U1F  $\beta$ -decay rates presented here can be important in determinations of the nucleosynthesis yields of the elements and their isotopes, both during hydrostatic burning regimes and the subsequent collapse and explosive burning phases. This microscopic calculation of U1F  $\beta$ -decay rates in stellar environment presented here is expected to prove quite useful for core-collapse simulator world-wide.

### **Acknowledgments**

The authors would like to acknowledge the support of the Horia Hulubei Foundation through the project IDEI-PCE, Contract No. 58/28.11.2011.

- 
- [1] H. V. Klapdor, Prog. Part. Nucl. Phys **10**,131 1983.
- [2] K. Grotz and H.V. Klapdor, The Weak Interaction in Nuclear, Particle and Astrophysics, Adam Hilger, Bristol, Philadelphia, New York, 1990.
- [3] G. McLaughlin and G. Fuller, Astrophys. J., **489**, 766 2000.
- [4] E.M. Burbidge, G.M. Burbidge, W.A. Fowler, F. Hoyle, Rev. Mod. Phys., **29**, 547 (1959)
- [5] J. Cooperstein and J. Wambach, Nucl. Phys. A **420**, 591 (1984).
- [6] M. B. Aufderheide, I. Fushiki, S. E. Woosley, E. Stanford, and D. H. Hartmann, Astrophys. J. Suppl. **91**, 389 (1994).
- [7] K. Langanke and G. Martínez-Pinedo, Rev. Mod. Phys., **75**, 819 (2003)
- [8] E.K. Warburton and J.A. Becker and D.J. Millener and B.A. Brown, Ann. Phys,**187**, 471 1988.
- [9] E.K. Warburton and I.S. Towner and B.A. Brown, Phys. Rev. C,**49**, 824 1994.
- [10] K. Takahashi, M. Yamada and T. Kondoh, At. Data Nucl. Data Tables, **12**, 101 1973.
- [11] A. Staudt, E. Bender, K. Muto and H. V.Klapdor-Kleingrothaus, At. Data. Nucl. Data Tables, **44**, 79 1990.
- [12] M. Hirsch, A. Staudt, K. Muto and H. V. Klapdor-Kleingrothaus, At. Data Nucl. Data Tables, **53**, 165 1993.
- [13] K.Muto, E. Bender and T. Oda, Phys. Rev. C, **43**, 1487 1991.
- [14] P. Möller, B. Pfeiffer and K.-L. Kratz, Phys. Rev. C, **67**, 055802 2003.
- [15] J. Engel, M. Bender, J. Dobaczewski, W. Nazarewicz and R. Surman, Phys. Rev. C, **60**, 014302 1999.
- [16] T. Niksic, T. Marketin, D. Vretenar, N. Paar and P. Ring, Phys. Rev. C, **71**, 014308 2005.
- [17] T. Marketin, D. Vretenar and P.Ring, Phys. Rev. C, **75**, 024304 2007.
- [18] V. Klapdor, J. Metzinger and T. Oda, At. Data. Nucl. Data Tables, **31**, 81 1984.
- [19] H. Homma, E. Bender, M. Hirsch, K. Muto, H. V. Klapdor-Kleingrothaus and T. Oda, Phys. Rev. C, **54**, 2972 1996.
- [20] K. Langanke and G. Martínez-Pinedo, Nucl. Phys. A **673**, 481 (2000).
- [21] J.-U. Nabi and H. V. Klapdor-Kleingrothaus, At. Data Nucl. Data Tables, **88**, 237 2004.
- [22] E.-W. Grewe *et. al.*, Phys. Rev. C, **78**, 044301 2008.
- [23] H. F. Schopper, Weak Interactions and Nuclear Beta Decay (North-Holland, Amsterdam, 1966).
- [24] C. S. Wu and S. A. Moszkowski, Beta Decay (Wiley, New York, 1966).
- [25] E. D. Commins, Weak Interactions (McGraw-Hill, NewYork, 1973).
- [26] J. M. Blatt and V. F. Weisskopf, Theoretical Nuclear Physics (Springer, Berlin, 1979).
- [27] H. Behrens and W. Bühring, Electron Radial Wave Functions and Nuclear Beta-Decay (Clarendon, Oxford, 1982).
- [28] K. Muto, E. Bender, T. Oda and H.V. Klapdor-Kleingrothaus, Z. Phys. A, **341**, 407 1992.
- [29] J.-U. Nabi and H. V. Klapdor-Kleingrothaus, At. Data. Nucl. Data Tables, **71**, 149 1999

- [30] P. Möller and J. R. Nix, *At. Data Nucl. Data Tables* **26**, 165 (1981).
- [31] G. Audi, A. H. Wapstra, and C. Thibault, *Nucl. Phys.* **A729**, 337 (2003).
- [32] N. B. Gove, M. J. Martin, *At. Data Nucl. Data Tables* **10**, 205 (1971).
- [33] S. Franchoo et al., *Phys. Rev. Lett.*, **81**, 3100 1998.
- [34] F. Ameil *et al.*, *Eur. Phys. J. A*,**1**, 275 1998.
- [35] P. T. Hosmer *et al.*, *Phys. Rev. Lett.* **94**, 112501 (2005).
- [36] I. N. Borzov, *Phys. Rev. C*, **71**, 065801 2005.
- [37] Vern L. Peterson and John N. Bahcall, *Astrophys. J.*,**138**,437 1963.

TABLE I: Comparison of calculated allowed and unique first-forbidden (U1F) phase space factors for  $^{72-78}\text{Ni}$  for different selected densities and temperatures in stellar matter. The first column gives stellar densities ( $\rho Y_e$ ) having units of  $\text{g}/\text{cm}^3$ , where  $\rho$  is the baryon density and  $Y_e$  is the ratio of the electron number to the baryon number. Temperatures ( $T_9$ ) are given in units of  $10^9$  K.

$\rho Y_e$	$T_9$	Phase space ( $^{72}\text{Ni}$ )		Phase space ( $^{73}\text{Ni}$ )		Phase space ( $^{74}\text{Ni}$ )		Phase space ( $^{75}\text{Ni}$ )		Phase space ( $^{76}\text{Ni}$ )		Phase space ( $^{77}\text{Ni}$ )		Phase space ( $^{78}\text{Ni}$ )	
		Allowed	U1F	Allowed	U1F	Allowed	U1F	Allowed	U1F	Allowed	U1F	Allowed	U1F	Allowed	U1F
$10^2$	0.01	1.7E+04	6.5E+04	9.3E+04	3.9E+05	8.1E+04	4.4E+05	4.0E+05	1.7E+06	1.9E+05	1.1E+06	4.3E+05	2.1E+06	3.4E+05	2.2E+06
	1	4.0E+08	1.0E+10	2.6E+08	1.4E+10	1.8E+08	3.2E+09	5.1E+08	9.9E+08	2.3E+08	1.8E+10	9.6E+08	1.3E+09	2.3E+08	4.9E+10
	3	4.0E+08	1.0E+10	2.6E+08	1.4E+10	1.8E+08	3.2E+09	5.1E+08	9.9E+08	2.3E+08	1.8E+10	9.6E+08	1.3E+09	2.3E+08	4.9E+10
	10	4.0E+08	1.0E+10	2.6E+08	1.4E+10	1.8E+08	3.2E+09	5.1E+08	9.9E+08	2.3E+08	1.8E+10	9.6E+08	1.3E+09	2.3E+08	4.9E+10
$10^6$	0.01	1.7E+04	6.5E+04	9.2E+04	3.9E+05	8.0E+04	4.4E+05	4.0E+05	1.7E+06	1.9E+05	1.1E+06	4.3E+05	2.1E+06	3.4E+05	2.2E+06
	1	4.0E+08	1.0E+10	2.6E+08	1.4E+10	1.8E+08	3.2E+09	5.1E+08	9.9E+08	2.3E+08	1.8E+10	9.6E+08	1.3E+09	2.3E+08	4.9E+10
	3	4.0E+08	1.0E+10	2.6E+08	1.4E+10	1.8E+08	3.2E+09	5.1E+08	9.9E+08	2.3E+08	1.8E+10	9.6E+08	1.3E+09	2.3E+08	4.9E+10
	10	4.0E+08	1.0E+10	2.6E+08	1.4E+10	1.8E+08	3.2E+09	5.1E+08	9.9E+08	2.3E+08	1.8E+10	9.6E+08	1.3E+09	2.3E+08	4.9E+10
$10^{10}$	0.01	0.0E+00	0.0E+00	0.0E+00	0.0E+00	0.0E+00	0.0E+00	0.0E+00	0.0E+00	0.0E+00	0.0E+00	0.0E+00	0.0E+00	0.0E+00	0.0E+00
	1	5.1E+07	2.3E+09	1.3E+07	6.6E+09	9.2E+06	1.1E+09	4.2E+07	3.2E+08	2.2E+07	8.0E+09	1.3E+08	5.4E+08	2.5E+07	2.5E+10
	3	5.2E+07	2.4E+09	1.3E+07	6.6E+09	9.7E+06	1.1E+09	4.3E+07	3.2E+08	2.3E+07	8.1E+09	1.4E+08	5.5E+08	2.5E+07	2.5E+10
	10	6.6E+07	2.8E+09	2.0E+07	6.9E+09	1.5E+07	1.2E+09	5.8E+07	3.5E+08	3.0E+07	8.4E+09	1.7E+08	5.7E+08	3.3E+07	2.6E+10

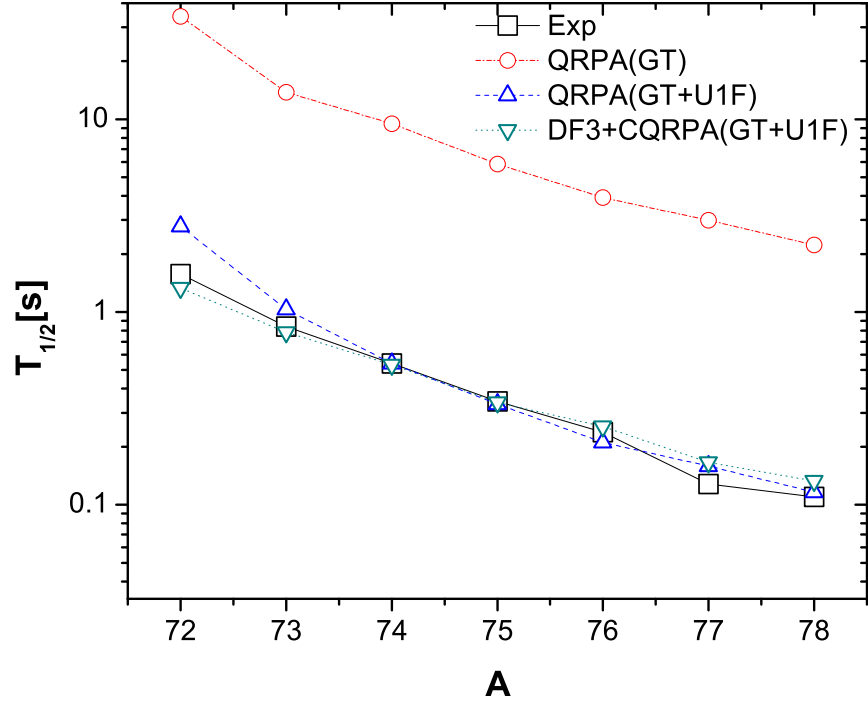


FIG. 1: Total  $\beta$ -decay half-lives for Ni isotopes calculated from the pn-QRPA (this work) including only the allowed (GT), allowed plus unique first-forbidden (GT+U1F) transitions, in comparison with the DF3+CQRPA [36] and experimental data [33–35].

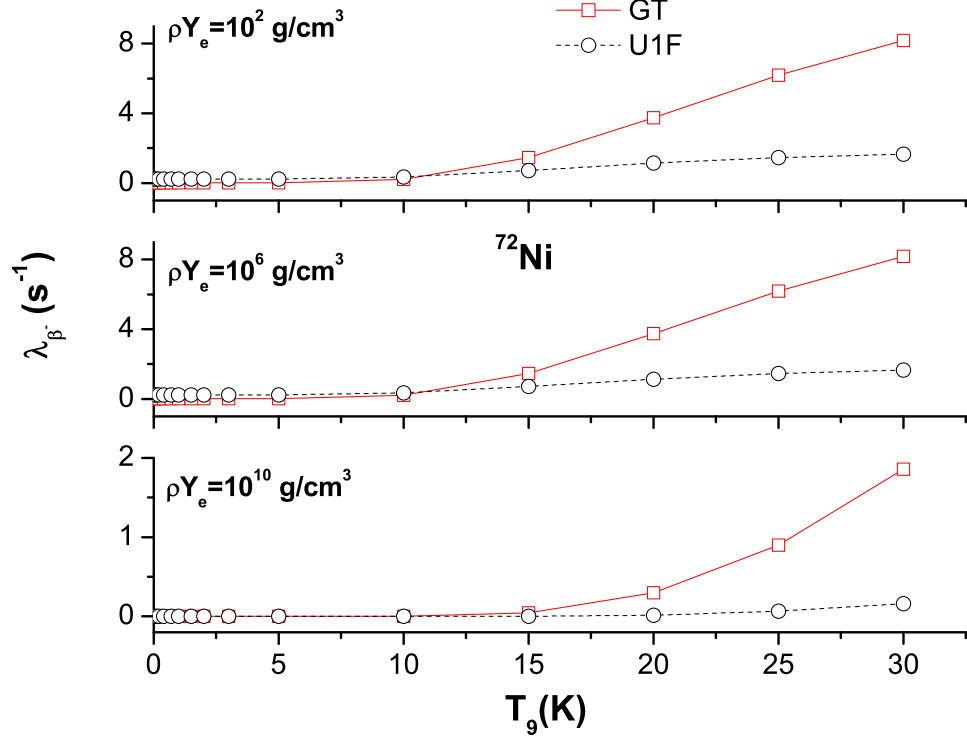


FIG. 2: Allowed (GT) and unique first-forbidden (U1F)  $\beta$ -decay rates on  $^{72}\text{Ni}$  as function of temperature for different selected densities. All  $\beta$  decay rates are given in units of  $\text{sec}^{-1}$ . Temperatures ( $T_9$ ) are given in units of  $10^9$  K.

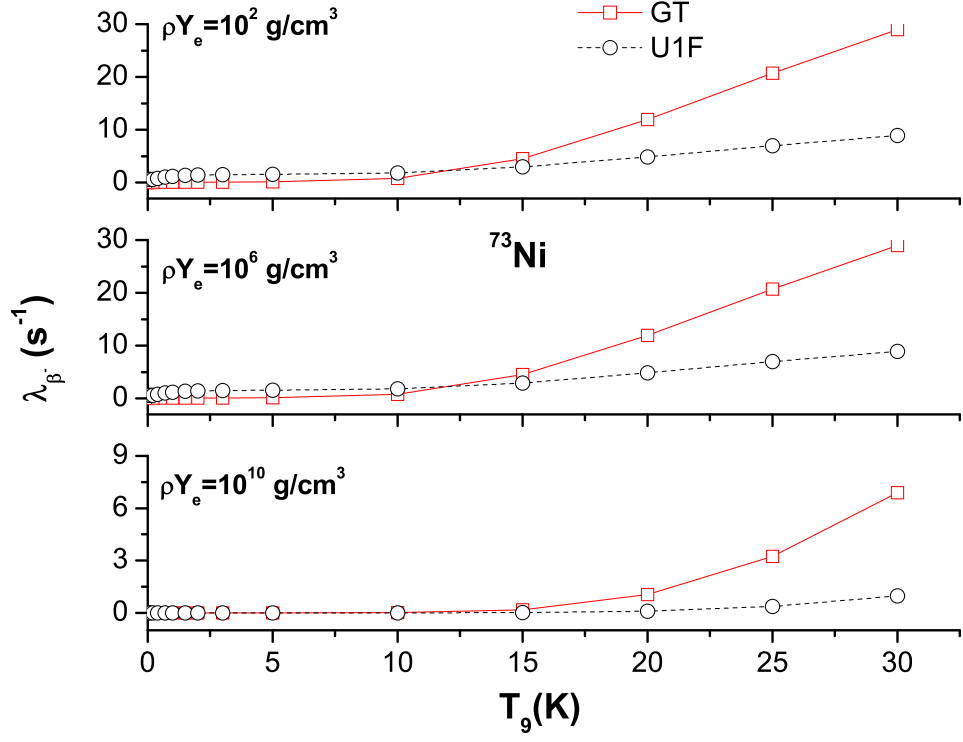


FIG. 3: Same as Fig. 2 but for  $^{73}\text{Ni}$



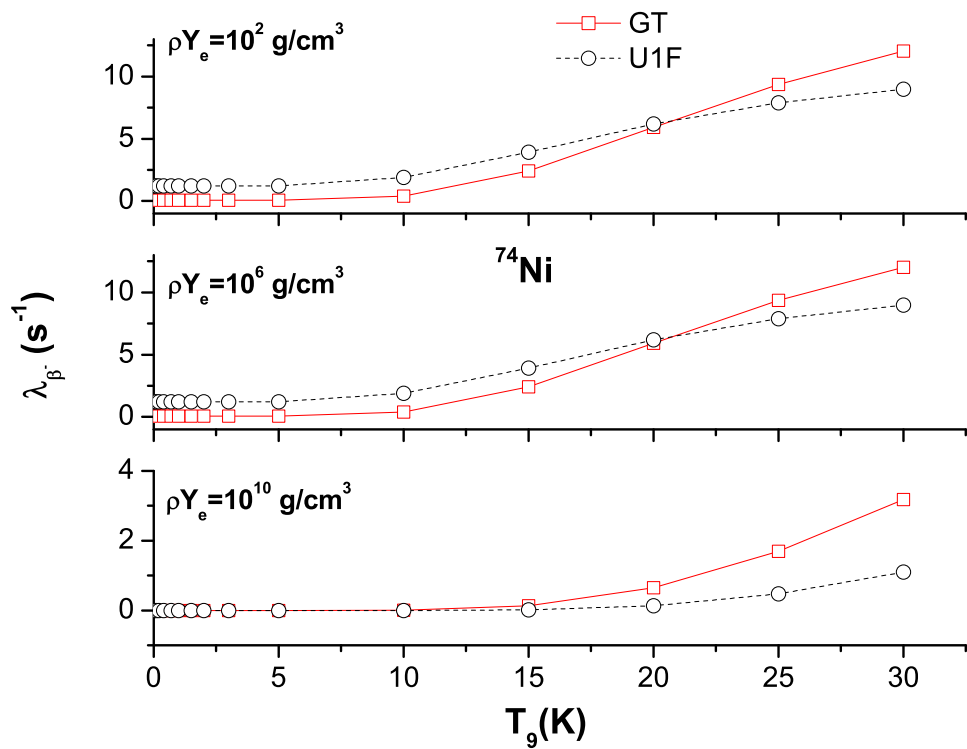


FIG. 4: Same as Fig. 2 but for  $^{74}\text{Ni}$

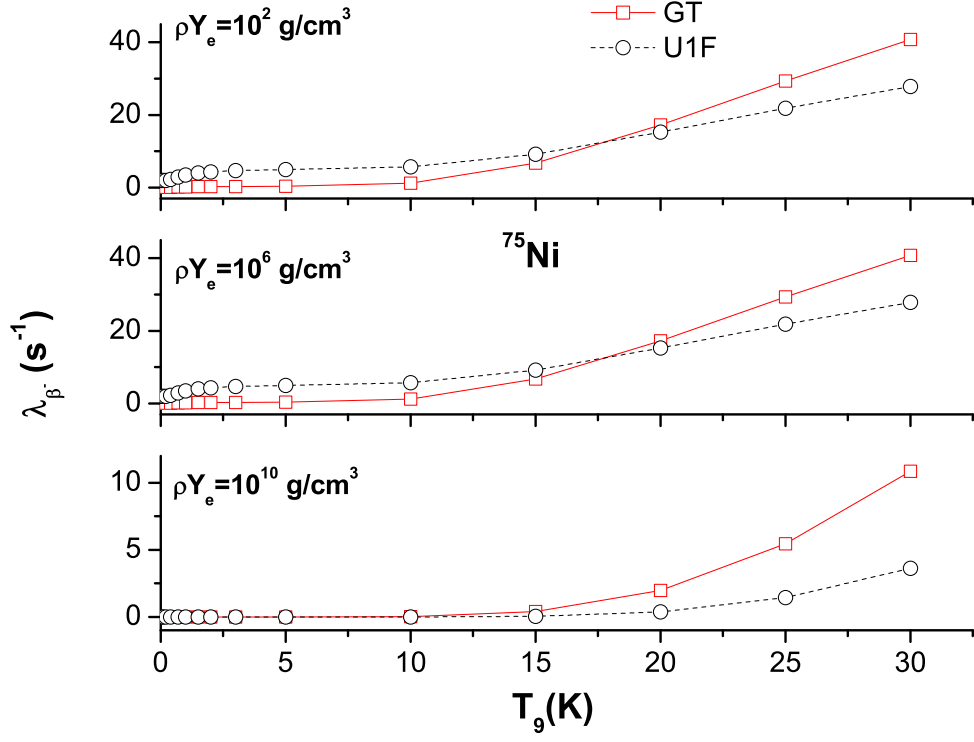


FIG. 5: Same as Fig. 2 but for  $^{75}\text{Ni}$

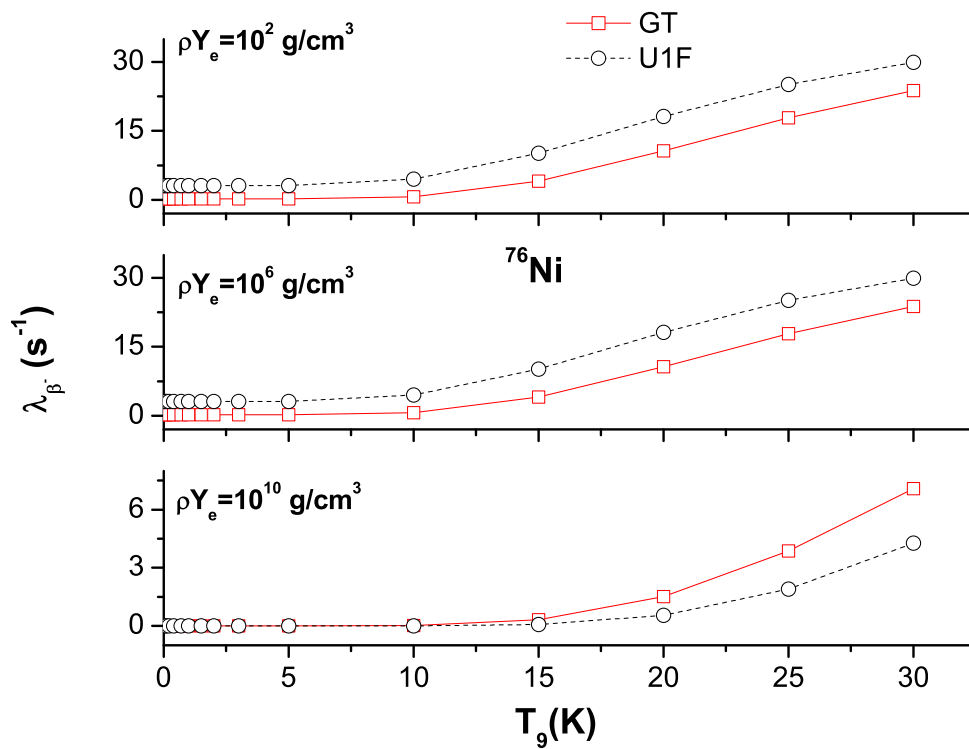


FIG. 6: Same as Fig. 2 but for  $^{76}\text{Ni}$

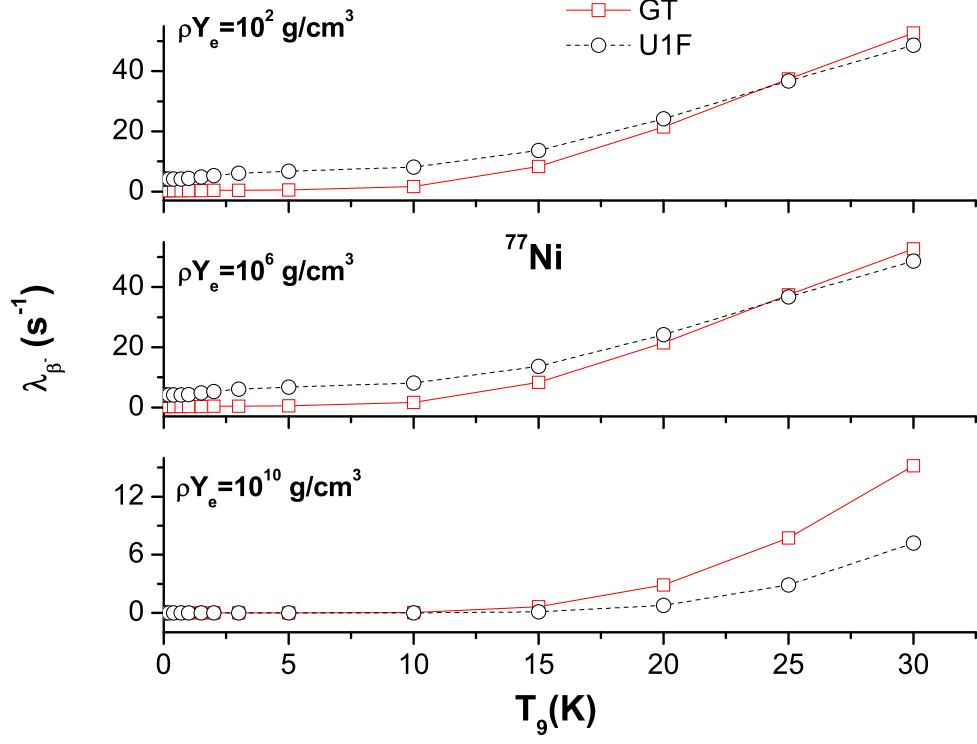


FIG. 7: Same as Fig. 2 but for  $^{77}\text{Ni}$

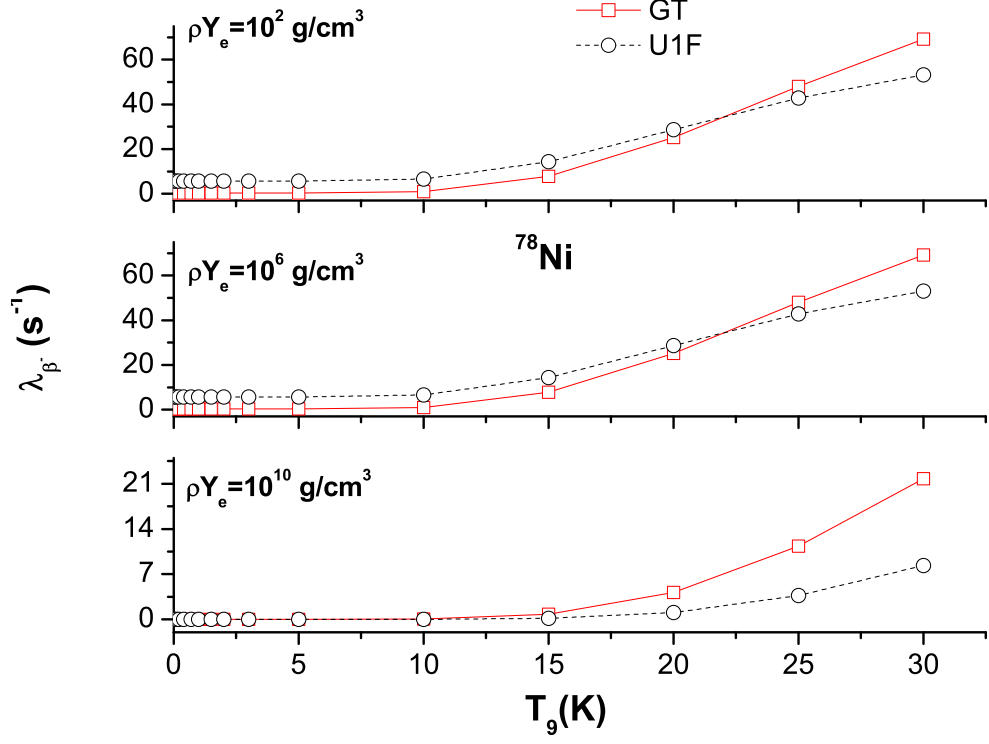


FIG. 8: Same as Fig. 2 but for  $^{78}\text{Ni}$